Eur. Phys. J. B **62**, 1–6 (2008)
DOI: 10.1140/epjb/e2008-00116-y

THE EUROPEAN PHYSICAL JOURNAL B

Experimental investigation on zero-$\emptyset_{\text{eff}}$ gaps of photonic crystals containing single-negative materials

Liwei Zhang[1], Yewen Zhang[1,2,a], Li He[1], Hongqing Li[1,2], and Hong Chen[1,2]

[1] Pohl Institute of Solid State Physics, Tongji University, Shanghai 200092, P.R. China
[2] School of Electronics and Information, Tongji University, Shanghai 200092, P.R. China

Received 3 May 2007 / Received in final form 18 January 2008
Published online 19 March 2008 –

Abstract. Epsilon-negative (ENG) and mu-negative (MNG) materials are successfully realized by using composite right/left-handed transmission line (CRLH TL), based on which the photonic crystals were also constituted. The simulated and measured scattering parameters and phase shift indicate that the photonic crystals containing single-negative (SNG) materials can possess zero-effective phase (zero-$\emptyset_{eff}$) gaps, which are insensitive to the scaling change of the respective unit length. The width and depth of zero-$\emptyset_{eff}$ gaps can be adjusted by varying the ratio of the length of ENG and MNG materials. The characteristics can be utilized to design a compact high quality factor (high-Q) filter, which is demonstrated by a defect mode in the photonic crystals in experiments.

PACS. 42.70.Qs Photonic bandgap materials – 78.20.Ci Optical constants – 41.20.Jb Electromagnetic wave propagation; radiowave propagation

1 Introduction

Periodic dielectric media called photonic crystals have attracted considerable attention in recent years [1]. Multilayered medium is considered as a simple example of one-dimensional photonic crystals (1DPCs). The essential property of PCs is the photonic band-gap (PBG) structure originated from the consequence of Bragg scattering. Such a Bragg gap in conventional PCs is strongly dependent on the lattice constant, the incident angle and the polarization of the electromagnetic (EM) wave. Besides, the width and depth of the Bragg gap depend on the materials and the size of the PCs. In order to obtain omnidirectional gaps beyond the Bragg scattering mechanism, zero-$\bar{n}$ gaps [2,3] and zero-$\emptyset_{eff}$ gaps [4–6] were presented, which are all invariant with scaling and disorder, and are insensitive to the incident angle for different polarization. Moreover, the edges of the peculiar gaps can be accurately determined by zero average permittivity $\bar{\varepsilon} = 0$ and zero average permeability $\bar{\mu} = 0$ for the case of normal incidence, respectively [7,8]. Zero-$\bar{n}$ gaps only exist in the layered structures combining positive-index materials and negative-index materials. It is usually shallow and not wide compared with zero-$\emptyset_{eff}$ gap which can appear in multilayers containing two different single negative (SNG) materials. Zero-$\emptyset_{eff}$ gap was first defined in reference [4], that is, once the effective phase shift (at wave impedance matching frequency) mismatched in the different SNG materials, a gap will open at zero effective phase delay point. The important feature of zero-$\emptyset_{eff}$ gap is that the band width and depth can be adjusted by varying the ratio of the two materials' thickness [4,7]. So zero-$\emptyset_{eff}$ gap can be controlled flexibly by the adjustment of the thickness ratio of layers and it has been used to design compact high quality factor (high-Q) filters [6] and zero-phase-shift omnidirectional filters [9] in theory.

The SNG materials [4,6,10,11] include epsilon-negative (ENG) materials ($\varepsilon < 0,\ \mu > 0$) and mu-negative (MNG) materials ($\varepsilon > 0,\ \mu < 0$). ENG materials can be realized by periodically arranged metallic wires [12] and MNG materials can be implemented by a periodic array of metallic split ring resonator (SRR) structures [13]. In a mismatched composite right/left-handed transmission line (CRLH TL) characterized by nonresonance, the single negative (SNG) materials can also be realized between left-handed passband and right-handed passband with low loss [14].

In this paper, SNG materials were physically realized by using CRLH TL, based on which the photonic crystals containing ENG and MNG materials were fabricated as in [15]. To realize the confinement effect of the photonic crystals, a defect needs to embed. The properties of the transmission are simulated by Advanced Design System (ADS) of Agilent and measured by the Agilent 8722ES vector network analyzer. The unique properties of zero-$\emptyset_{eff}$ gaps will allow novel applications and RF/microwave devices, such as compact high-Q filters, to be developed. The experimental results agree extremely well with the simulations.

[a] e-mail: yewenzhang@online.sh.cn

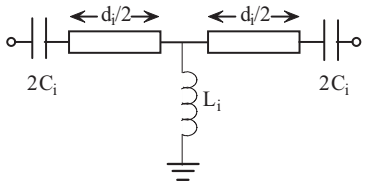

Fig. 1. The schematic and circuit model of a CRLH TL unit with the loading lumped element series capacitors (C_i) and shunt inductor (L_i).

2 Experiment and simulation

Figure 1 is the proposed unit cell of the CRLH TL. The structure constituted of a host TL medium with the distributed parameters L_0 and C_0 and the discrete loading lumped element components, L and C. The CRLH TL fabricated by the (periodic or not) repetition of the unit cell with small average electric length ($d_i < \lambda_g/4$) is effectively homogeneous in a certain range of frequencies [16]. It exhibits effective – uniformity behaviour rigorously expressed with the constitutive parameters ε and μ, where d_i is the average cell size, λ_g is guided wavelength. For a CRLH TL which is a quasi-transverse electromagnetic (TEM) waveguide, the constitutive parameters can be obtained by mapping the telegrapher equations to Maxwell equations [17], the effectively relative ε and μ are given by the following approximate expressions,

$$\varepsilon_i \approx \left(C_0 - \frac{1}{(2\pi f)^2 L_i d_i}\right)/(\varepsilon_0 \cdot p),$$
$$\mu_i \approx p \cdot \left(L_0 - \frac{1}{(2\pi f)^2 C_i d_i}\right)/\mu_0, \quad (1)$$

where p is a structure constant, $i = 1, 2$ denotes the different type of CRLH TL. For a mismatched CRLH TL, the distinct characteristic is that it exhibits a band structure with two evident passbands and stopbands. Expressions for the pertinent cutoff frequency f_1 and eigenfrequencies f_2 and f_3 are as follows [18]:

$$f_1 = \frac{1}{4\pi\sqrt{L_i C_i}},\ f_2 = \frac{1}{2\pi\sqrt{C_0 L_i d_i}},\ f_3 = \frac{1}{2\pi\sqrt{L_0 C_i d_i}} \quad (2)$$

the lower frequency range between f_1 and f_2 is left-handed (LH), the upper frequency range is right-handed (RH), the stopband displaying between f_2 and f_3 is either ENG or MNG in nature, depending on the CRLH TL parameters. For convenience, ENG TL and MNG TL are introduced to describe the CRLH TLs which possess ENG or MNG in a certain range of frequencies, respectively. For ENG TL, the eigenfrequency $f_2 > f_3$, while for MNG TL, the eigenfrequency $f_2 < f_3$.

ENG TL and MNG TL have been made by FR-4 substrate with a thickness of $h = 1.6$ mm, relative permittivity of $\varepsilon_{sub} = 4.75$, relative permeability $\mu_{sub} = 1.0$ and the structure constant $p \approx 4.05$. Based on the ENG TL and MNG TL units, photonic crystals were also constructed as in [15]. In ENG TL, 50 Ω TLs were designed to have unit length of $d_1 = 6$ mm, the loading lumped element components $L_1 = 5.6$ nH, $C_1 = 5.1$ pF, and in MNG TL, $d_2 = 8$ mm, $L_2 = 10$ nH and $C_2 = 1$ pF, respectively. From about 0.8 GHz to 6.0 GHz, ENG TL and MNG TL can be regarded as effectively homogeneous media with different permittivity and permeability since $d_i = \lambda_g/4$ is the homogeneity limit [19].

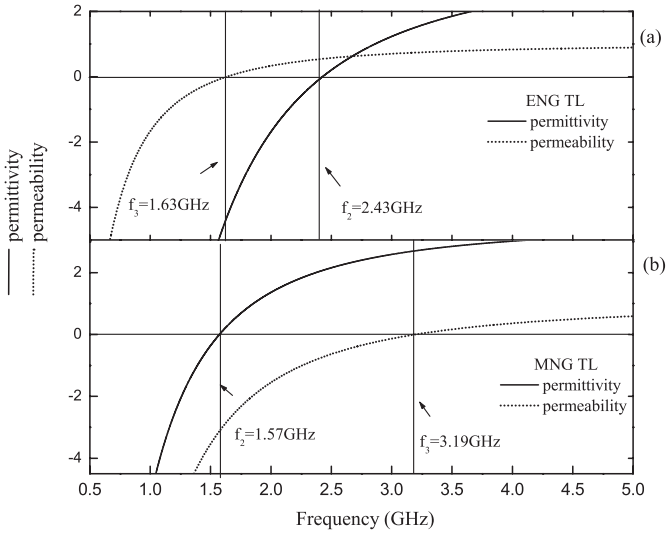

Fig. 2. The calculated relative permittivity (ε) and permeability (μ) of the ENG TL (a) where the eigenfrequency $f_2 > f_3$ and MNG TL (b) where the eigenfrequency $f_2 < f_3$ based on ideal lumped element components, respectively.

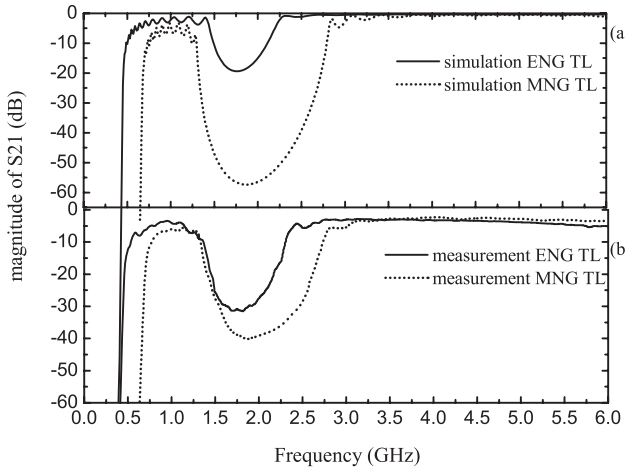

Fig. 3. The simulated and measured scattering parameters of the proposed ENG TL (a) and MNG TL (b) using real lumped element components, respectively.

The calculated relative permittivity and permeability of the ENG TL and MNG TL according to equation (1) gave in Figures 2a and 2b respectively. It shows clearly that the SNG frequency range for ENG TL is 1.63–2.43 GHz, and the frequency range, where $\mu < 0$ and $\varepsilon > 0$ for MNG TL is 1.57–3.19 GHz.

Figures 3a and 3b show the simulated and measured scattering parameters of ENG TL and MNG TL based on real lumped element components respectively. With respect to ENG TL containing sixteen CRLH TL units, the cutoff frequency and eigenfrequencies of the simulated

Fig. 4. Photographs of the fabricated photonic crystals, $(ENG_1MNG_1)_{12}$ (a), $(ENG_2MNG_2)_6$ (b), and $(ENG_3MNG_3)_4$ (c) based on CRLH TLs, respectively.

results are about 0.46 GHz, 1.46 GHz and 2.18 GHz, 0.7 GHz, 1.28 GHz and 2.8 GHz for MNG TL which comprised of twelve CRLH TL units, respectively. There are some deviations in comparison with the calculated values shown in Figure 2 due to the difference between the ideal and real lumped element components. The experimental measurements agree well with the simulations. On the whole, ENG TL and MNG TL are all SNG materials over the frequencies 1.46–2.18 GHz in our experiments.

The photonic crystals formed by stacking alternate ENG layers and MNG layers can be a equivalent left-handed material if the wave impedance and the effective phase shift of ENG and MNG materials are under the conditions of match, respectively [11,15]. Otherwise, the photonic crystals will possess zero-$Ø_{eff}$ gap [4,5] which open at the zero phase delay point. It is insensitive to a change of scale length, and the gap width can be adjusted by changing the ratio of ENG and MNG materials' unit length in theory. To demonstrate the special gap's characteristics of the periodic structures cascaded by ENG materials with MNG materials in experiment, we fabricated five kinds of one-dimensional photonic crystals with $(ENG_1MNG_1)_{12}$, $(ENG_2MNG_2)_6$, $(ENG_3MNG_3)_4$, $(ENG_2MNG_1)_8$ and $(ENG_1MNG_2)_8$, where the subscripts "1", "2" and "3" represent the number of ENG TL and MNG TL units in one period, "12", "8", "6" and "4" represent the period, respectively. The photographs of the fabricated photonic crystals $(ENG_1MNG_1)_{12}$, $(ENG_2MNG_2)_6$ and $(ENG_3MNG_3)_4$ are shown in Figure 4, we do not show the photographs of $(ENG_2MNG_1)_8$ and $(ENG_1MNG_2)_8$ since they are similar in outside.

Figure 5a shows the ADS simulated transmission properties of the photonic crystals, $(ENG_1MNG_1)_{12}$, $(ENG_2MNG_2)_6$ and $(ENG_3MNG_3)_4$. These structures are typical photonic crystals structures, so the Bragg gaps will exist, and the frequencies must scale with the lattice constant. The center frequencies of the Bragg gaps shown in the figure increase with the unit length in lower frequency, while decrease in high frequency band. In the SNG frequency for the ENG TL and MNG TL, there exists an unconventional gap. In the three kinds of photonic crystals, the gaps exhibit around 2.0 GHz which do not vary with the unit length and differ from the Bragg gaps in the left-handed range and right-handed range. It implies that the unconventional gap is zero-$Ø_{eff}$ gap. Figure 5b shows the measured scattering parameters, the experimental results coincide with the simulations. Figures 6a and 6b are the simulated and measured phase delay of $(ENG_1MNG_1)_{12}$, $(ENG_2MNG_1)_8$ and $(ENG_1MNG_2)_8$ respectively, good agreement between them can be observed. The figure clearly illustrates that the phase shift of the three kinds of photonic crystals equal zero at the same frequency point in the special gap.

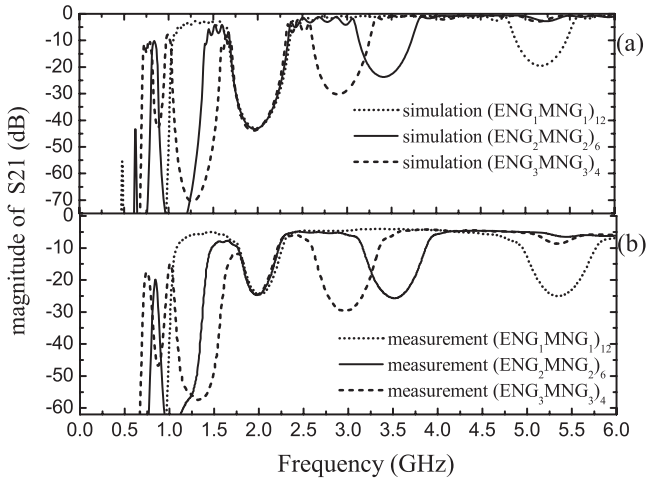

Fig. 5. The simulated (a) and measured (b) scattering parameters of the photonic crystals, $(ENG_1MNG_1)_{12}$, $(ENG_2MNG_2)_6$ and $(ENG_3MNG_3)_4$ based on CRLH TLs using real lumped element components, respectively.

Figure 7 shows the simulated and measured transmission of $(ENG_1MNG_1)_{12}$, $(ENG_2MNG_1)_8$ and $(ENG_1MNG_2)_8$, which agree well with each other. It clearly highlights that the width and depth of zero-$Ø_{eff}$ gaps vary with the ratio of the length of ENG and MNG units. Compared to the photonic crystals $(ENG_1MNG_1)_{12}$ and $(ENG_2MNG_1)_8$, $(ENG_1MNG_2)_8$ possesses the widest and deepest zero-$Ø_{eff}$ gap.

For a defect embedded in a 1DPCs, it will result in discrete defect modes inside the PBG due to the confinement effect, and lead to the filtering phenomenon. The

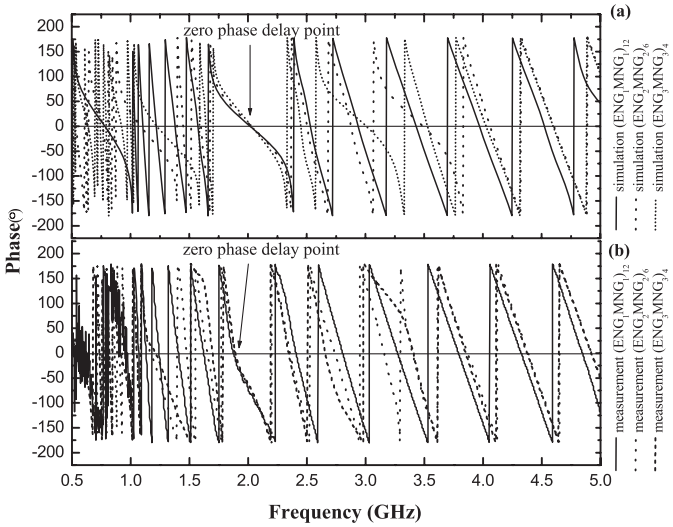

Fig. 6. The simulated (a) and measured (b) phase delay of the photonic crystals $(ENG_1MNG_1)_{12}$, $(ENG_2MNG_2)_6$ and $(ENG_3MNG_3)_4$ based on CRLH TLs using real lumped element components, respectively.

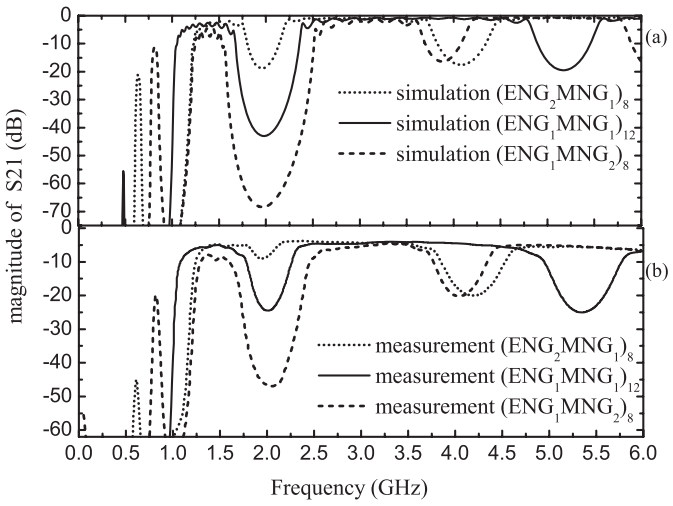

Fig. 7. The simulated (a) and measured (b) scattering parameters of the photonic crystals, $(ENG_1MNG_1)_{12}$, $(ENG_2MNG_1)_8$ and $(ENG_1MNG_2)_8$ based on CRLH TLs using real lumped element components, respectively.

wider and deeper gap will benefit to improve the quality factor. According to the characteristic of zero-$\emptyset_{eff}$ gap, compact high quality factor (high-Q) filters can be designed as presented in [6]. In the method, the quality factor can increase by adjusting the ratio of respective unit length, while the volume of this kind of filter reduces. Figure 8 presents the prototypes of two kinds of filters in the form of $(ENG_2MNG_2)_3Z(MNG_2ENG_2)_3$ and $(ENG_1MNG_2)_3Z(MNG_2ENG_1)_3$ based on a defect in 1DPCs with the same structures. The symbol Z stands for a 50 Ω microstrip transmission line with a length of $d = 20$ mm, working as a defect. The performances of the two kinds of filters based on real lumped element components shown in Figure 9. It explicitly reveals that a microstrip line defect resulted in defect modes at about 2.03 GHz in the two kinds of filters respectively, the FWHM (Full Width at Half Maximum) of the defect mode and out-of-band rejection are different. In comparison with $(ENG_2MNG_2)_3Z(MNG_2ENG_2)_3$, $(ENG_1MNG_2)_3Z(MNG_2ENG_1)_3$ has smaller volume, narrower FWHM and high out-of-band rejection. The measured results are consistent with the simulations. The features are propitious to design compact high-Q filters, on the other hand, zero-phase-shift omnidirectional filters can also be achieved in the photonic heterostructures ground on zero-$\emptyset_{eff}$ gaps [9].

3 Discussion

In order to further understand the results measured above, we analyze the transmission of the photonic crystals consisting of ENG and MNG materials with the help of transfer-matrix method [2,20]. As far as the ENG materials and MNG materials based on a lossless CRLH TL are concerned, the effective relative permittivity and permeability according to equation 1 can be described as

$$\varepsilon_A = \varepsilon_\alpha - \frac{\alpha_A}{(2\pi f)^2},\ \mu_A = \mu_\alpha - \frac{\beta_A}{(2\pi f)^2} \tag{3}$$

for ENG materials and

$$\varepsilon_B = \varepsilon_\beta - \frac{\alpha_B}{(2\pi f)^2},\ \mu_B = \mu_\beta - \frac{\beta_B}{(2\pi f)^2} \tag{4}$$

for MNG materials, where A and B represent ENG and MNG materials respectively, f is the frequency measured in GHz, $\varepsilon_{\alpha(\beta)}$ and $\mu_{\alpha(\beta)}$ are constant determined by the host microstip line. $\alpha_{A(B)}$ and $\beta_{A(B)}$ are the circuit parameters that can be modulated with the loading lumped element components, series capacitors (C_i), shunt inductors (L_i) and the unit length (d_i). The unit length of ENG and MNG materials are assume to be d_A and d_B, respectively. For the specific parameters used in experimental circuits shown in Figure 1, $\varepsilon_{\alpha(\beta)} = 3.57$, $\alpha_A = 830.4$, $\mu_{\alpha(\beta)} = 1.0$, $\beta_A = 105.3$, $d_A = 6$ mm and $\alpha_B = 348.7$, $\beta_B = 4015$, $d_B = 8$ mm. For the periodic structures composed of ENG and MNG materials in the form of $(AB)_{12}$, $(A_2B_2)_6$ and $(A_3B_3)_4$, the effective wave impedance $\eta_{A(B)}$ and the effective phase shift $\Phi_{A(B)}$ in each layer can be written as

$$\eta_{A(B)} = \sqrt{|\mu_{A(B)}\mu_0\,(\varepsilon_{A(B)}\,\varepsilon_0)|} \tag{5}$$

$$\Phi_{A(B)} = k_0\sqrt{|\varepsilon_{A(B)}\,\mu_{A(B)}|}d_{A(B)} \tag{6}$$

the wave number in each layer can be written as

$$k_{A(B)} = k_0\sqrt{\varepsilon_{A(B)}\,\mu_{A(B)}} \tag{7}$$

respectively [4], where k_0 is the wave number in vacuum. The phase-match condition $\Phi_A = \Phi_B$ at the wave impedance match frequency $(\eta_A = \eta_B)$ decides whether

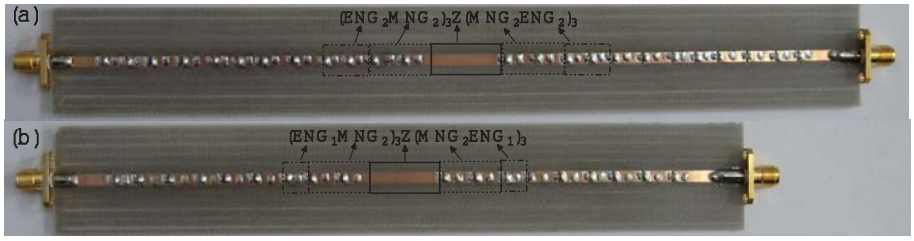

Fig. 8. Prototypes of the fabricated filters based on photonic crystals containing a microstrip line defect, $(ENG_2MNG_2)_3Z(MNG_2ENG_2)_3$(a) and $(ENG_1MNG_2)_3Z(MNG_2ENG_1)_3$ (b) based on CRLH TLs, respectively.

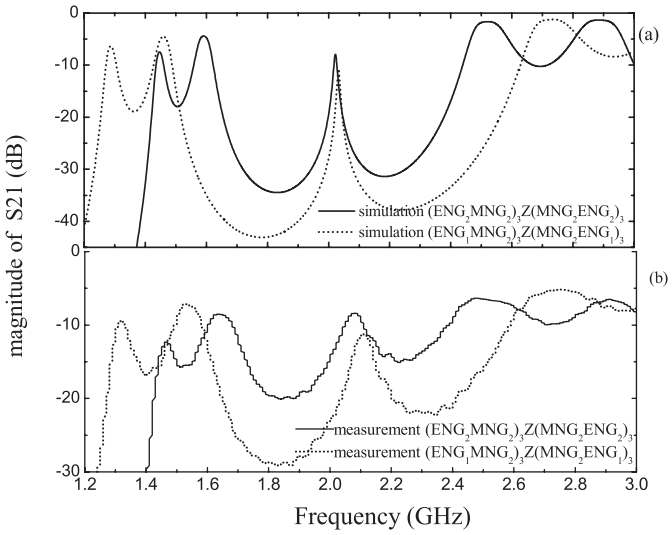

Fig. 9. The simulated (a) and measured (b) scattering parameters of the fabricated filters $(ENG_2MNG_2)_3Z(MNG_2ENG_2)_3$, $(ENG_1MNG_2)_3Z(MNG_2ENG_1)_3$ using real lumped element components, respectively.

the photonic crystals possess propagation modes within all the SNG frequency range [11,15]. Otherwise, the photonic crystals exhibit zero-$\emptyset_{eff}$ gap within the SNG frequency range, it is another new type of photonic gaps except zero-$\bar{n}$ gap [3]. The important feature of the zero-$\emptyset_{eff}$ gaps is that it is insensitive to the incident angle and the wave polarizations, invariant upon the changes of scale length. The gap width and depth can be altered by changing the ratio of the unit length of ENG and MNG materials. Moreover, it is surrounded by left-handed propagation modes and the right-handed propagation modes, and the edges of the gap are almostly determined by $\bar{\varepsilon} = 0$ and $\bar{\mu} = 0$ respectively [7]. In accordance with the parameters chosen in equations (3) and (4), the effective phase of ENG and MNG materials in the three kinds of photonic crystals $(AB)_{12}$, $(A_2B_2)_6$ and $(A_3B_3)_4$ do not match in a certain frequency range, therefore the photonic crystals possess zero-$\emptyset_{eff}$ gaps. The peculiar gaps will be independent of a change of scale length in the SNG for A and B. Whereas, for the Bragg gaps of the photonic crystals as shown in Figure 4, the center frequencies vary with the unit length and the trend is opposite in low frequency range and high frequency band respectively, which satisfy the condition [21],

$$k'_A d_A + k'_B d_B = m\pi \tag{8}$$

where $k'_{A(B)}$ is the real part of the respective wave number and m is the band-gap index which can be any integer, including zero and negative numbers. According to the dispersion characteristics of A and B, the center frequency of the Bragg gaps will increase with the thickness of each layer $(d_{A(B)})$ when m is negative integer, and the gaps exist in the left-handed passband for A or B. When m greater than zero, the Bragg gaps appear in the right-handed passband for A or B, and the center frequency will decrease with the thickness of each layer by reason of the condition in equation (8).

Figures 10a–10c show the calculated transmission of $(AB)_{12}$, $(A_2B_2)_6$ and $(A_3B_3)_4$ for the case of normal incidence, respectively. When $m = -1$, the center frequencies of the Bragg gaps are about 1.2 GHz, 1.7 GHz and 1.85 GHz for $(AB)_{12}$, $(A_2B_2)_6$ and $(A_3B_3)_4$ respectively, increasing with the thickness of each layer, which is different from that of $m = 1$ in high frequencies band. Between the frequencies 1.95–2.7 GHz, a spectral gap called zero-$\emptyset_{eff}$ gaps appear, which do not shift when the unit length is multiplied by two and three times. Around the gaps, propagation modes formed in the photonic crystals due to the interaction of the interface mode based on evanescent modes or propagation modes. The characteristics of the propagation modes in the photonic crystals depend essential on the average permittivity $(\bar{\varepsilon} = (\varepsilon_A d_A + \varepsilon_B d_B)/(d_A + d_B))$ and average permeability $(\bar{\mu} = (\mu_A d_A + \mu_B d_B)/(d_A + d_B))$. Figure 10d shows the calculated $\bar{\varepsilon}$ and $\bar{\mu}$ of the photonic crystals, $\bar{\varepsilon}$ and $\bar{\mu}$ approximately equal zero at 1.95 GHz and 2.7 GHz respectively, $\bar{\varepsilon}$ and $\bar{\mu}$ are both negative when frequency $f < 1.95$ GHz, positive when $f > 2.7$ GHz. The photonic crystals can be regarded as effective SNG materials between the frequency regions 1.95–2.7 GHz, where the product of $\bar{\varepsilon} \cdot \bar{\mu} < 0$ and the zero-$\emptyset_{eff}$ gaps exist. The spectral gaps of the three kinds of photonic crystals stay almost at the same frequency region shown in Figures 10a–10c in that $\bar{\varepsilon}$ and $\bar{\mu}$ are maintained when the ratio of unit numbers keep a constant. If change the ratio of the thickness of respective SNG materials, $\bar{\varepsilon}$ and $\bar{\mu}$ will vary. Subsequently, the effective SNG frequency band will vary, that is, the width and depth of zero-$\emptyset_{eff}$ gaps were adjusted by the thickness ratio. For the $(ENG_1MNG_2)_8$ structure, the range

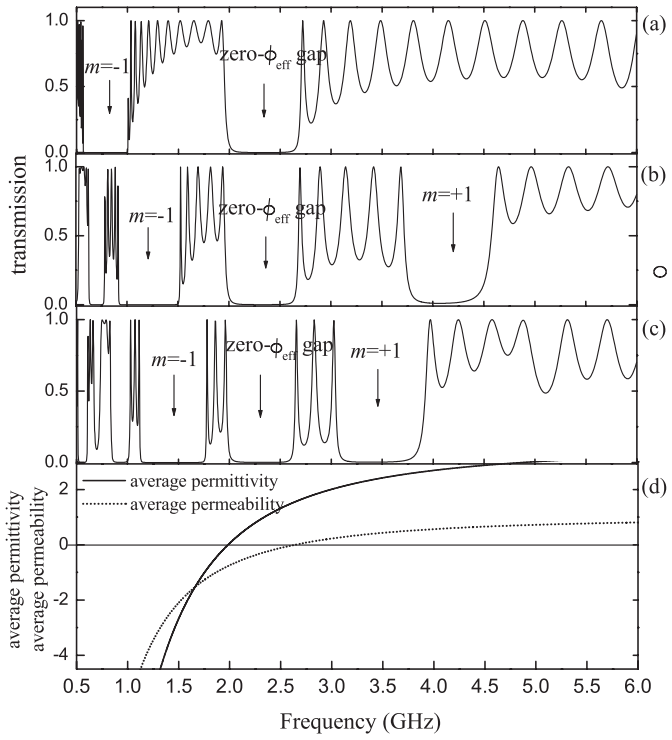

Fig. 10. The calculated transmission of the photonic crystals $(AB)_{12}$ (a), $(A_2B_2)_6$ (b), $(A_3B_3)_4$ (c), where m is the band-gap index, (d) shows the average permittivity ($\bar{\varepsilon}$) and the average permeability ($\bar{\mu}$) of the photonic crystals.

of $\bar{\varepsilon} \cdot \bar{\mu} < 0$ is wider and the value of $|\bar{\varepsilon} \cdot \bar{\mu}|$ is bigger than that of $(ENG_1MNG_1)_{12}$ and $(ENG_2MNG_1)_8$ in the SNG frequency for ENG and MNG materials. So the $(ENG_1MNG_2)_8$ structure possesses much wider and deeper zero-$\emptyset_{eff}$ gaps as shown in Figure 7. For the defect mode in a PBG, the FWHM descend with the confinement effect which is directly determined by the gap width and depth. Usually, the wider and deeper the gap, the larger the quality factor of the filter. The merit of zero-$\emptyset_{eff}$ gap is to fabricate high-Q filter while decreasing the volume by choosing appropriate length ratio. As for the two kinds of filters with the same structure presented in Figure 8, the second filter has relative higher quality factor but smaller volume, the interesting filtering phenomenon can be well explained by the wider and deeper effective SNG gap.

4 Conclusion

The photonic crystals consisting of ENG and MNG materials are fabricated by using CRLH TL, which possess zero-$\emptyset_{eff}$ gaps. Experimentally, zero-$\emptyset_{eff}$ gaps are invariant with a change of scale length, and the gap width and depth can be adjusted by changing the length ratio of respective materials. It is theoretically show that in zero-$\emptyset_{eff}$ gaps, the photonic crystals can be regarded as an effective SNG material, the characteristic of zero-$\emptyset_{eff}$ gap can contribute to the compact high quality factor filters.

This research was supported by National Basic program (973) of China (No. 2006CB921701), by the National Natural Science Foundation of China (No. 10634050) and by Shanghai Committee of Science and Technology (No. 07DZ22302).

References

1. E. Yablonovitch, Phys. Rev. Lett. **58**, 2059 (1987)
2. H.T. Jiang, H. Chen, H.Q. Li, Y.W. Zhang, Appl. Phys. Lett. **83**, 5386 (2003)
3. J. Li, L. Zhou, C.T. Chan, P. Sheng, Phys. Rev. Lett. **90**, 083901 (2003)
4. H.T. Jiang, H. Chen, H.Q. Li, Y.W. Zhang, J. Zi, S.Y. Zhu, Phys. Rev. E **69**, 066607 (2004)
5. L.G. Wang, H. Chen, S.Y. Zhu, Phys. Rev. B **70**, 245102 (2004)
6. H.T. Jiang, H. Chen, H.Q. Li, Y.W. Zhang, S.Y. Zhu, J. Appl. Phys. **98**, 013101 (2005)
7. L. Gao, C.J. Tang, S.M. Wang, J. Magn. Magn. Mater. **301**, 371 (2006)
8. L. W. Zhang, Y. W. Zhang , L. He, Z. G. Wang, H. Q. Li, and H. Chen, J. Phys. D: Appl. Phys. **40**,2579 (2007)
9. G.G. Guan, H.T. Jiang, H.Q. Li, Y.W. Zhang, H. Chen, Appl. Phys. Lett. **88**, 211112 (2006)
10. D.R. Fredkin, A. Ron, Appl. Phys. Lett. **81**, 1753 (2002)
11. A. Al, N. Engheta, IEEE Trans. Antennas Propagat. **51**, 2558 (2003)
12. J.B. Pendry, A.J. Holden, D.J. Robbins, W.J. Stewart, J. Phys. Condens. Matter. **10**, 4785 (1998)
13. J.B. Pendry, A.J. Holden, D.J. Robbins, W.J. Stewart, IEEE Trans. Microwave Theory Tech. **47**, 2075 (1999)
14. T. Fujishige, C. Caloz, T. Itoh, Microwave Opt. Technol. Lett. **46**, 476 (2005)
15. L.W. Zhang, Y.W. Zhang, L. He, H.Q. Li, H. Chen, Phys. Rev. E. **74**, 056615 (2006)
16. N. Engheta, R.W. Ziolkowski, *Metamaterials Physics, Engineering Explorations* (Wiley, New York, 2006)
17. G.V. Eleftheriades, A.K. Iyer, P.C. Kremer, IEEE Trans. Microwave Theory Tech. **50**, 2702 (2002)
18. M.A. Antoniades, G.V. Eleftheriades, IEEE Antennas Wireless Propagat. Lett. **72**, 103 (2003)
19. C. Caloz, T. Ioh, *Electromagnetic Metamaterials, Transmission Line Theory, Microwave Applications* (Wiley, IEEE Press, 2005)
20. N.H. Liu, S.Y. Zhu, H. Chen, X. Wu, Phys. Rev. E **65**, 046607 (2003)
21. R. Ruppin, Microwave Opt. Technol. Lett. **38**, 494 (2003)